# Differentiation of Brain Infection From Necrotic Glioblastoma Using Combined Analysis of Diffusion and Perfusion MRI

Sanjeev Chawla, PhD,[1†]* Sumei Wang, MD,[1†] Suyash Mohan, MD, PDCC,[1] MacLean Nasrallah, MD, PhD,[2] Gaurav Verma, PhD,[1] Steven Brem, MD,[3] Donald M. O'Rourke, MD,[3] Ronald L. Wolf, MD, PhD,[1] Harish Poptani, PhD,[4] and S. Ali Nabavizadeh, MD[1]

**Background:** Accurate differentiation of brain infections from necrotic glioblastomas (GBMs) may not always be possible on morphologic MRI or on diffusion tensor imaging (DTI) and dynamic susceptibility contrast perfusion-weighted imaging (DSC-PWI) if these techniques are used independently.
**Purpose:** To investigate the combined analysis of DTI and DSC-PWI in distinguishing brain injections from necrotic GBMs.
**Study Type:** Retrospective.
**Population:** Fourteen patients with brain infections and 21 patients with necrotic GBMs.
**Field Strength/Sequence:** 3T MRI, DTI, and DSC-PWI.
**Assessment:** Parametric maps of mean diffusivity (MD), fractional anisotropy (FA), coefficient of linear (CL), and planar anisotropy (CP) and leakage corrected cerebral blood volume (CBV) were computed and coregistered with postcontrast $T_1$-weighted and FLAIR images. All lesions were segmented into the central core and enhancing region. For each region, median values of MD, FA, CL, CP, relative CBV (rCBV), and top 90$^{th}$ percentile of rCBV ($rCBV_{max}$) were measured.
**Statistical Tests:** All parameters from both regions were compared between brain infections and necrotic GBMs using Mann–Whitney tests. Logistic regression analyses were performed to obtain the best model in distinguishing these two conditions.
**Results:** From the central core, significantly lower MD ($0.90 \times 10^{-3} \pm 0.44 \times 10^{-3}$ mm$^2$/s vs. $1.66 \times 10^{-3} \pm 0.62 \times 10^{-3}$ mm$^2$/s, $P = 0.001$), significantly higher FA ($0.15 \pm 0.06$ vs. $0.09 \pm 0.03$, $P < 0.001$), and CP ($0.07 \pm 0.03$ vs. $0.04 \pm 0.02$, $P = 0.009$) were observed in brain infections compared to those in necrotic GBMs. Additionally, from the contrast-enhancing region, significantly lower rCBV ($1.91 \pm 0.95$ vs. $2.76 \pm 1.24$, $P = 0.031$) and $rCBV_{max}$ ($3.46 \pm 1.41$ vs. $5.89 \pm 2.06$, $P = 0.001$) were observed from infective lesions compared to necrotic GBMs. FA from the central core and $rCBV_{max}$ from enhancing region provided the best classification model in distinguishing brain infections from necrotic GBMs, with a sensitivity of 91% and a specificity of 93%.
**Data Conclusion:** Combined analysis of DTI and DSC-PWI may provide better performance in differentiating brain infections from necrotic GBMs.
**Level of Evidence:** 1
**Technical Efficacy:** Stage 2

J. MAGN. RESON. IMAGING 2019;49:184–194.

Differentiation of patients with brain infection from those with necrotic glioblastoma (GBM) can present a diagnostic challenge. Expedient and accurate distinction between these conditions would be very important, as these entities have different clinical courses and management strategies.[1] Brain infections can be potentially cured,[2] unless

View this article online at wileyonlinelibrary.com. DOI: 10.1002/jmri.26053

Received Jan 12, 2018, Accepted for publication Mar 28, 2018.

*Address reprint requests to: S.C., Senior Research Investigator, Department of Radiology, Perelman School of Medicine at the University of Pennsylvania, Philadelphia, PA 19104. E-mail: Sanjeev.Chawla@uphs.upenn.edu

From the [1]Department of Radiology, Perelman School of Medicine at the University of Pennsylvania, Philadelphia, Pennsylvania, USA; [2]Department of Pathology and Lab Medicine, Perelman School of Medicine at the University of Pennsylvania, Philadelphia, Pennsylvania, USA; [3]Department of Neurosurgery, Perelman School of Medicine at the University of Pennsylvania, Philadelphia, Pennsylvania, USA; and [4]Department of Cellular and Molecular Physiology, University of Liverpool, Liverpool, UK

†The first two authors contributed equally to this work.

 

appropriate treatment is delayed.[3] On the other hand, necrotic GBMs usually require detailed presurgical planning aiming at maximal safe surgical resection. Moreover, overdiagnosis of a necrotic GBM carries a burden of psychosocial ramifications for a patient. However, in view of nonspecific clinical symptoms, and equivocal findings on conventional magnetic resonance imaging (MRI),[4,5] it is often a challenging task to accurately distinguish brain infections from necrotic GBMs.

Multiple studies[6–13] have reported a promising role of diffusion and perfusion MRI in studying intracranial masses. Using diffusion-weighted imaging (DWI), some studies[7,10,12] have reported significantly lower mean diffusivity (MD) from the central core of brain infections compared to those of necrotic GBMs. However, high diffusivity similar to that found in necrotic high-grade gliomas has also been reported in 5–21% of abscesses.[14–16] In addition, necrotic GBMs with low MD values in the central core have also been reported,[10,17] increasing the conundrum about the utility of DWI in differentiating the two entities. Some studies using diffusion tensor imaging (DTI) reported that infective lesions demonstrate high fractional anisotropy (FA) mimicking necrotic GBMs,[9,18,19] suggesting that differential diagnosis may not always be possible on the basis of diffusion imaging alone.

Dynamic susceptibility contrast perfusion-weighted imaging (DSC-PWI) has also been used in differentiating infective from neoplastic lesions.[6,7] However, some investigators reported a significantly decreased cerebral blood volume (CBV) from contrast-enhancing regions of infective lesions compared to those of necrotic neoplastic lesions,[6,7,11,13] while others[20,21] have observed similar patterns of CBV in these two types of cystic lesions. Taken together, these studies suggest that the use of diffusion or perfusion imaging alone may not always provide accurate differentiation of brain infections and necrotic GBMs.

In one study, Chan et al[6] used both DWI and DSC-PWI to differentiate brain infections from necrotic gliomas. However, these two techniques were used independently and imaging parameters derived from these techniques were not synergistically integrated to obtain a reliable classification model. Additionally, comprehensive analysis of DTI data provides additional parameters such as linear and planar anisotropy coefficients (CL and CP) describing characteristics of tensor shape, and thus further elucidating tissue characterization. Using a combined analytical approach of incorporating DTI and PWI data, numerous studies[22–25] have reported characterization of different types of brain tumors as well as distinction of patients with true progression from pseudoprogression exemplifying the importance of a combining the DTI and DSC-PWI analysis.

Therefore, the purpose of the current study was to evaluate the potential utility of combined analysis of DTI and DSC-PWI in differentiating brain infections from necrotic GBMs.

## Materials and Methods

### Patients

This retrospective study was approved by the Institutional Review Board and was compliant with the Health Insurance Portability and Accountability Act. The primary inclusion criteria for patients were as follows: 1) one or more cystic/necrotic lesions with rim-like enhancement on postcontrast $T_1$-weighted images, 2) no prior treatment with corticosteroids, antibiotics, or antifungal therapy. The exclusion criteria included large areas of susceptibility associated with enhancing lesions substantially degrading image quality for generation of diffusion and perfusion metrics employed in multiparametric assessment.

Based on the inclusion and exclusion criteria, a cohort of 35 patients with different brain pathologies were included in this study. The final diagnosis of the disease was confirmed by histological and microbiological analyses of a collected fluid/tissue specimen following surgical intervention (aspiration/stereotactic biopsy/surgical resection). These patients were divided into two groups. In the first group, 14 patients (mean age standard deviation = 50.2 ± 13.3 years, males/females = 10/4) with brain infections were included. Of these 14 patients, 12 showed negative serology for human immunodeficiency virus infection. In all cases, causative microorganisms were established, whereby eight cases were determined to be pyogenic abscess, four were confirmed for fungal abscess, one had toxoplasma abscess, and the remaining one patient had tuberculoma, who showed no overt focus of infection in the lungs. One patient with fungal abscess had two lesions, while all other patients had a solitary lesion. Therefore, a total of 15 different lesions from brain infections were considered while analyzing the data. The demographic characteristics and etiological findings from this group of patients are summarized in Table 1. The second group comprised 21 patients with necrotic GBMs (mean ± standard deviation = 58.4 ± 12.2 years, males/females = 12/9). All these patients had a single lesion. The locations of necrotic GBMs were as follows: frontal ($n = 5$); parietal ($n = 4$); temporal ($n = 6$); occipital ($n = 2$); fronto-parietal ($n = 2$); fronto-temporal ($n = 1$); parieto-occipital ($n = 1$).

### MRI

All Patients underwent MRI on a 3T Tim Trio whole body MR scanner (Siemens, Erlangen, Germany) equipped with a 12-channel phased array head coil. The anatomical imaging protocol included a 3-plane scout localizer, sagittal 3D $T_1$-weighted magnetization-prepared rapid acquisition of gradient echo (MPRAGE) imaging (repetition time [TR] / echo time [TE] /inversion time [TI] = 1620/3.9/950 msec); matrix size = 192 × 256; section thickness = 1 mm; number of sections per slab = 192; flip angle = 15°; number of excitations (NEX) = 1; bandwidth (BW) = 150 Hz/pixel), and an axial $T_2$-FLAIR image (TR/TE/TI = 9420/141/2500 msec); section thickness = 3 mm; number of sections = 60; flip angle = 170°; NEX = 1; BW = 287 Hz/pixel. The postcontrast $T_1$-weighted images were acquired with the same parameters as the precontrast acquisition after administration of gadobenate dimeglumine (MultiHance, Bracco Imaging, Milano,

**TABLE 1. Demographic Characteristics and Etiological Findings From Brain Infection Patients**

| Patient ID | Gender/ age (years) | Number of lesions | Location of lesions | Brain infection/ abscess | Surgical intervention | Etiological microorganism |
|---|---|---|---|---|---|---|
| 1 | M/53 | 1 | Frontal | Pyogenic | Pus aspiration | Gram-positive Cocci |
| 2 | M/57 | 1 | Frontal | Pyogenic | Surgery | Fusobacterium nucleatum |
| 3 | F/66 | 1 | Parietal | Pyogenic | Surgery | Gram-positive Cocci |
| 4 | M/53 | 1 | Thalamus | Pyogenic | Surgery | Coagulation negative staph |
| 5 | F/24 | 1 | Thalamus | Tuberculoma | Stereotactic biopsy | Mycobacterium tuberculosis |
| 6 | M/57 | 1 | Temporal | Pyogenic | Surgery | Streptococcus intermedius |
| 7 | M/55 | 2 | Bilateral Frontal | Fungal | Surgery | Aspergillus niger |
| 8 | M/43 | 1 | Lentiform nucleus | Toxoplasmosis | Medical Treatment | Toxoplasma gondii |
| 9 | F/58 | 1 | Frontal | Pyogenic | Surgery | Streptococcus anginosus |
| 10 | M/62 | 1 | Pons | Fungal | Stereotactic biopsy | Aspergillus fumigatus |
| 11 | F/22 | 1 | Frontal | Pyogenic | Surgery | Streptococcus intermedius |
| 12 | M/40 | 1 | Frontal | Fungal | Stereotactic biopsy | Histoplasma |
| 13 | M/55 | 1 | Parietal | Pyogenic | Surgery | Streptococcus anginosus |
| 14 | M/58 | 1 | Frontal | Fungal | Surgery | Cladophialophora bantiana |

Italy) intravenous contrast agent using a power injector (Medrad, Idianola, PA).

### DTI

DTI data were acquired using 30 noncollinear/noncoplanar directions with a single-shot spin-echo, echo-planar read-out sequence with parallel imaging by using generalized autocalibrating partially parallel acquisition (GRAPPA) and acceleration factor of 2. The sequence parameters were as follows: TR/TE = 5,000/86ms, NEX = 3, field of view (FOV) = 22 × 22 $cm^2$, matrix size = 128 × 128, in-plane resolution = 1.72 × 1.72 $mm^2$; slice thickness = 3 mm; b = 0, 1000 s/$mm^2$, number of slices = 40.

### PWI

For DSC-PWI, a bolus of contrast agent was injected with a preloading dose of 0.07 mmol/kg, which was utilized to reduce the effect of contrast agent leakage on CBV measurements. For DSC-PWI, $T_2$*-weighted gradient-echo EPI was performed during the second 0.07 mmol/kg bolus of contrast agent. The injection rate was 5 ml/s for all patients and was immediately followed by a bolus injection of saline (total of 20 ml at the same rate). The sequence parameters were as follows: TR/TE = 2000/45 msec; FOV = 22 × 22 $cm^2$; matrix size = 128 × 128; in-plane resolution = 1.72 × 1.72 $mm^2$; slice thickness = 3 mm; BW = 1346 Hz/pixel; flip angle = 90°; EPI factor = 128; echo spacing = 0.83. Forty-five sequential measurements were acquired for each section. $T_2$-FLAIR images were obtained after the preloading dose of contrast agent.

### Image Processing

The diffusion-weighted images were coregistered to the nondiffusion-weighted (b = 0) images from the DTI acquisition to minimize the artifacts induced by eddy currents and/or subject motion by using a 3D-affine transformation estimated by maximizing the mutual information between the images as described earlier.[24] The corrected raw images were combined to estimate the DTI parametric maps by using in-house developed algorithm

(IDL; ITT Visual Information Solutions, Boulder, CO).[24] Pixel-wise MD, FA, CL, and CP maps were computed. Additionally, leakage-corrected CBV maps using the $\gamma$-variate function were generated from DSC-PWI data by using NordicICE software (NordicNeuroLab, Bergen, Norway).

The scalar DTI, CBV maps, and FLAIR images were coregistered to contrast-enhanced $T_1$-weighted images. Using contrast-enhanced $T_1$ and FLAIR images, a semiautomatic segmentation approach was used to subdivide each lesion into two regions: the central core and enhancing region. Briefly, one region of interest (ROI) was drawn over the FLAIR abnormality on every section to create a 3D composite mask. Similarly, another mask was drawn on the contrast-enhanced $T_1$-weighted images in the contralateral normal white matter (WM). The enhancing region was defined as the region with enhancement higher than mean +3 standard deviations of the signal intensity from the WM. The nonenhancing area inside the enhancing region was defined as the central core.

The median values of DTI metrics (MD, FA, CL, and CP) and CBV from the central core and enhancing region were computed for each lesion. The CBV values from these two regions were normalized by corresponding values from contralateral normal WM regions to obtain relative CBV (rCBV). In addition, the 90$^{th}$ percentile of rCBV values were estimated from both regions. Instead of maximum rCBV value, the 90$^{th}$ percentile of rCBV was used to represent a hot spot of a lesion to avoid the outlier and noise effect. Using histogram analysis, a previous study[26] demonstrated that only the 90$^{th}$ percentile of rCBV was significantly correlated with cellular proliferation and microvascular density in high-grade gliomas. Hence, 90$^{th}$ percentile of rCBV was used in the present study and was considered $rCBV_{max}$. Previously,[24,25] we reported 90$^{th}$ percentile of rCBV in characterizing different brain tumors with high accuracy.

Additionally, conventional MRI characteristics were evaluated to differentiate brain infections from necrotic GBMs. The following characteristics were assessed: 1) homogeneous vs. heterogeneous signal intensity pattern from the central core of lesions as visible on $T_2$-FLAIR images; 2) normalized $T_1$ signal intensity from contrast enhancing region of lesions with respect to contralateral WM on postcontrast $T_1$-weighted images; 3) volume of the central core + enhancing region of lesions; and 4) volume of entire hyperintense $T_2$-FLAIR abnormality encompassing the lesions.

### *Statistical Analysis*

Mann–Whitney *U*-tests were performed to look for differences in median values of MD, FA, CL CP, rCBV, and $rCBV_{max}$ from the central core and enhancing region of lesions between patients with brain infections and necrotic GBMs. Additionally, conventional imaging characteristics such as normalized $T_1$ signal intensity from contrast enhancing regions and volumes were compared using Mann–Whitney *U*-tests and signal intensity pattern from the central core of lesions on $T_2$-FLAIR were compared using the chi-square test between two groups of patients. A probabilistic (*P*) vale of less than 0.05 was considered significant. To evaluate the potential utility of combined analysis of two techniques, all DTI and DSC-PWI parameters with a high predictive power ($P < 0.20$, Wald test) using univariate analysis were selected and incorporated into multivariate logistic regression analyses to determine the best classification model. To evaluate the goodness of fit for the best model, the Hosmer–Lemeshow test was performed. Additionally, a leave-one-out crossvalidation approach was applied to estimate the accuracy of the model. The receiver operating characteristic (ROC) analyses were performed by using the selected parameters and the output of the logistic regression model. Optimal cutoff values that maximize the Youden's index were determined. Sensitivity, specificity, and area under the ROC curve (AUC) were computed. In order to evaluate the performance of only DTI parameters (MD, FA, CL, and CP from the central core and enhancing region), logistic regression and ROC analyses were performed to determine the best DTI model in distinguishing brain infections from necrotic GBMs. Similar analyses using only DSC-PWI parameters (rCBV and $rCBV_{max}$ from the central core and enhancing region) were performed to determine the best DSC-PWI model. All statistical analyses were performed using a statistical package, SPSS for Windows (v. 18.0; Chicago, IL).

## Results

Representative anatomical images, MD, FA, CL, CP, and CBV maps, each from a patient with pyogenic abscess, fungal abscess, and necrotic GBM, are shown in Figs. 1–3, respectively. The distributions of median values of MD, FA, CL, CP, rCBV, and $rCBV_{max}$ from the central core and enhancing region of brain infections and necrotic GBMs are shown as box-whisker plots in Figs. 4 and 5, respectively.

From the central core, significantly lower MD were observed from infective lesions compared to those of necrotic GBMs (mean $\pm$ standard deviation $= 0.90 \times 10^{-3} \pm 0.44 \times 10^{-3}$ mm$^2$/s vs. $1.66 \times 10^{-3} \pm 0.62 \times 10^{-3}$ mm$^2$/s, $P = 0.001$). Additionally, significantly higher FA ($0.15 \pm 0.06$ vs. $0.09 \pm 0.03$, $P < 0.001$) and CP ($0.07 \pm 0.03$ vs. $0.04 \pm 0.02$, $P = 0.009$) were observed in infective lesions than in necrotic GBMs. However, no significant differences ($P > 0.05$) in CL, rCBV, and $rCBV_{max}$ were observed between two types of lesions. Interestingly, CP was significantly ($P < 0.05$) greater than CL from the central core, both in brain infections and in necrotic GBMs.

From the contrast-enhancing region, significantly lower rCBV ($1.91 \pm 0.95$ vs. $2.76 \pm 1.24$, $P = 0.031$) and $rCBV_{max}$ ($3.46 \pm 1.41$ vs. $5.89 \pm 2.06$, $P = 0.001$) were observed from infective lesions compared with necrotic GBMs. However, no significant differences ($P > 0.05$) in other parameters were observed between two types of lesions. Another interesting finding was that fungal abscesses (number of lesions = 5) had nonsignificant ($P > 0.05$) higher $rCBV_{max}$ ($4.56 \pm 1.98$ vs. $3.12 \pm 0.89$) than pyogenic abscesses (number of lesions = 8). Moreover, two fungal abscesses demonstrated $rCBV_{max}$ greater than the average of $rCBV_{max}$ from all necrotic GBMs.

Among parameters that showed high predictive power ($P < 0.2$, Wald test), FA from the central core was the single best predictor for distinguishing brain infections from necrotic GBM with an accuracy (AUC) of 0.86, a moderate

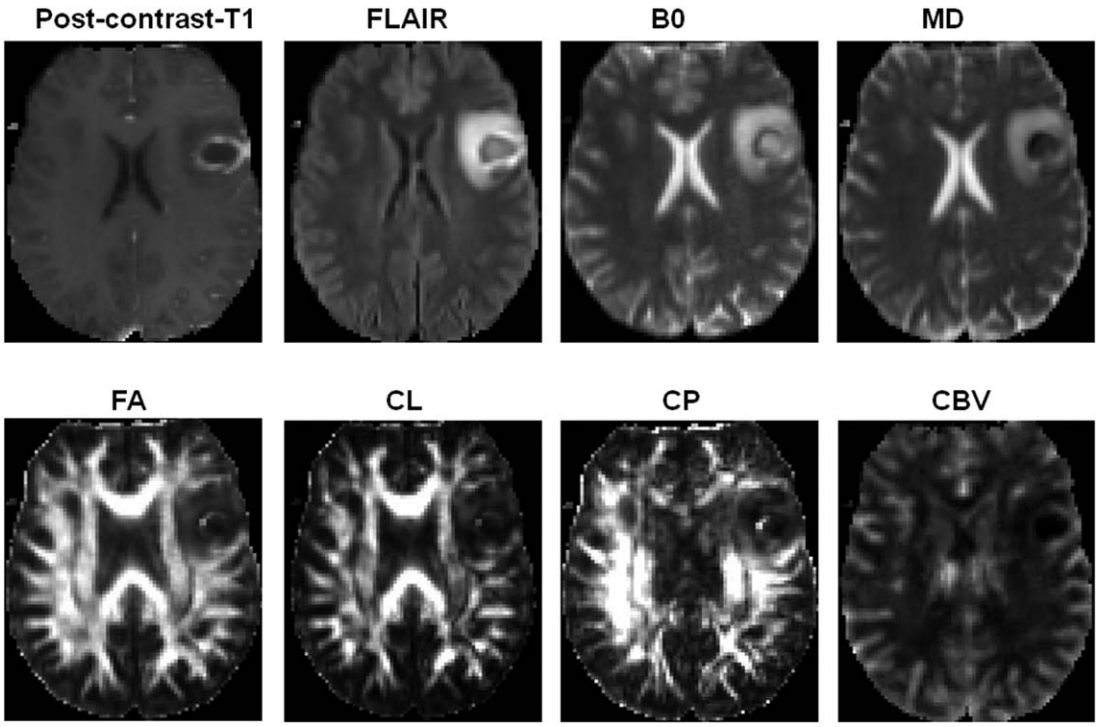


FIGURE 1: A 22-year-old patient with pyogenic abscess. An axial postcontrast $T_1$-weighted image demonstrating a ring-enhancing lesion in the left frontal lobe. This lesion demonstrates heterogeneous signal intensities on the corresponding FLAIR and $B_0$ images, with moderate edema. The central core of the lesion shows low signal on MD map, and slightly high signal intensities on FA and CP maps, indicating anisotropic content. An enhancing region in the abscess wall demonstrates minimally elevated rCBV.

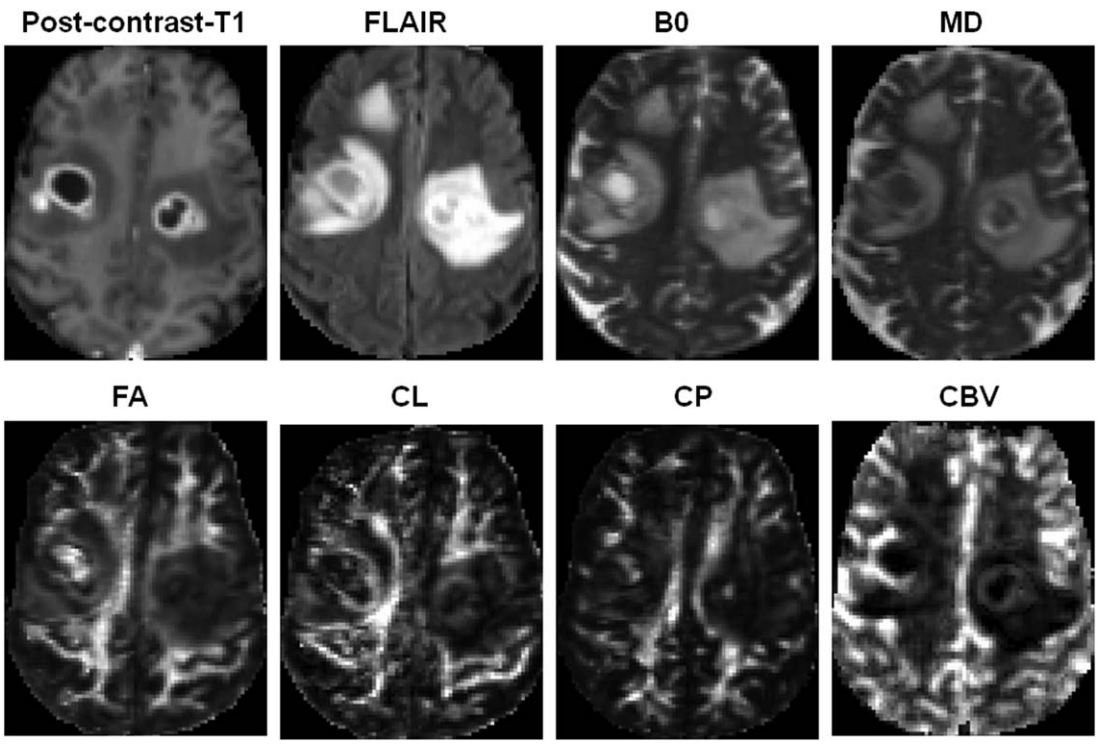


FIGURE 2: A 55-year-old patient with fungal abscesses. Axial postcontrast $T_1$-weighted image shows two ring-enhancing lesions, one in each hemisphere. Both of these lesions show heterogeneous signal intensities on the corresponding FLAIR and $B_0$ images and moderate to marked surrounding edema. The central core of the right lesion shows decreased MD and markedly increased FA, CL, and CP. Also, marked elevation of rCBV corresponding to the enhancing region is visible. The left lesion demonstrates mixed diffusivity from the central core but less striking increase in FA, CL, and CP, and milder elevation of rCBV from enhancing region.

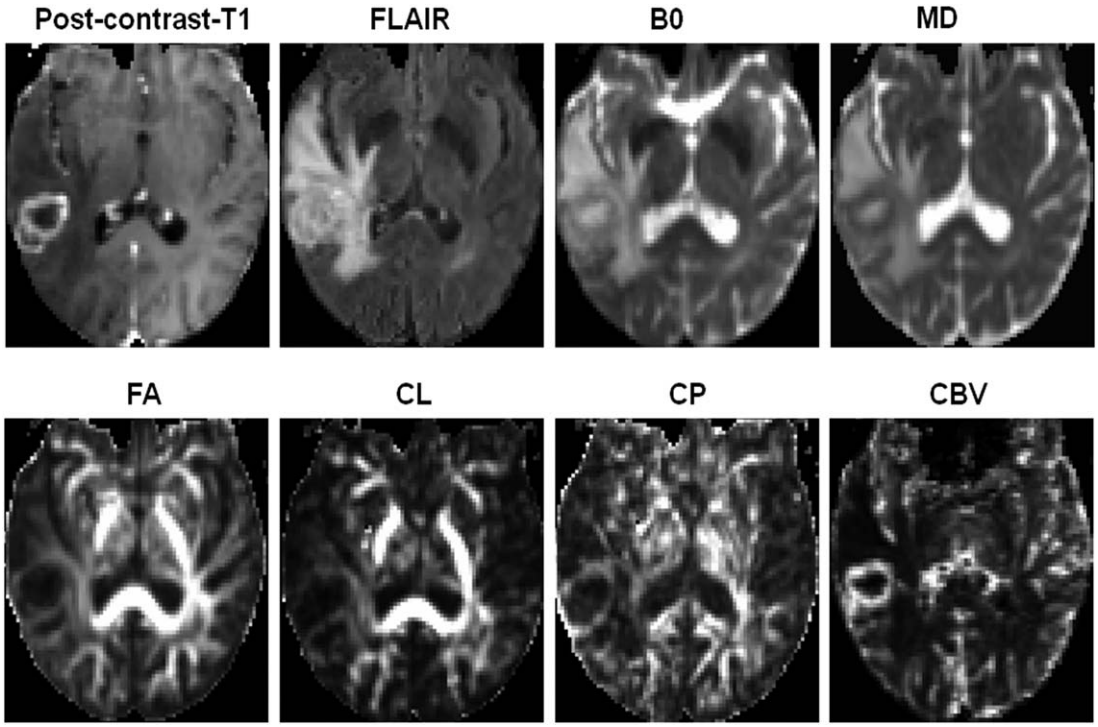


**FIGURE 3: A 58-year-old patient with necrotic GBM. Axial postcontrast $T_1$-weighted image demonstrates a ring-enhancing lesion in the right posterior temporal lobe, with heterogeneous signal intensities on the corresponding FLAIR and $B_0$ images as well as marked surrounding edema. The central core of the lesion shows high MD and low FA, CL, and CP. Also, marked elevation of rCBV corresponding to the enhancing region is visible.**

sensitivity of 67%, and a specificity of 93% using a threshold FA value of 0.09. Using multivariate logistic regression analyses, FA from the central core and $rCBV_{max}$ from enhancing regions were the best parameters that were selected in a backward stepwise method as follows:

$$f[FA(central\ core), rCBVmax(enhancing\ region) = 1/1+\exp[-(\beta 0+\beta 1FA+\beta 2rCBVmax)]$$

where $\beta_0 = 1.50$, $\beta_1 = -59.01$, and $\beta_2 = 1.18$. This classification model distinguished brain infections from necrotic GBMs with an accuracy (AUC) of 0.95, a sensitivity of 91%, and a specificity of 93% (Fig. 6). The summary of sensitivity and specificity for individual parameters and for the best classification model in distinguishing brain infections and necrotic GBMs is presented in Table 2. A $\chi^2$ value of 4.83 and a $P$ value of 0.68 were obtained from the Hosmer–Lemeshow test, reflecting an acceptable fit for the multivariate logistic regression model. Leave-one-out cross-validation tests revealed that 88.6% of patients were correctly classified as brain infection and necrotic GBM groups by discriminatory model.

When only DTI parameters were incorporated into logistic regression analyses, MD and FA from the central core and CP from enhancing region were selected in the backward stepwise method. This classification model distinguished brain infections from necrotic GBMs with an accuracy of 0.92, a sensitivity of 82%, and a specificity of 91%. On the other hand, when only DSC-PWI parameters were used in logistic regression analyses, $rCBV_{max}$ from the central core and rCBV and $rCBV_{max}$ from enhancing region were selected in the backward stepwise method. This classification model distinguished brain infections from necrotic GBMs with an accuracy of 0.90, a sensitivity of 81%, and a specificity of 86%.

### *Conventional MRI Characteristics*

More number of lesions with brain infections (6/15, 40%) had homogeneous signal intensity from the central core on $T_2$-FLAIR images than those with necrotic GBMs (6/21, 28.6%). However, this finding was not significant ($P = 0.47$). In spite of large variations observed in both types of lesions, volume of the central core + enhancing region in brain infections ($12.9 \pm 16.3\,cm^3$) was significantly ($P = 0.02$) smaller than that of necrotic GBMs ($25.7 \pm 13.3\,cm^3$). ROC analysis revealed a sensitivity of 66% and a specificity of 80%. However, volume of hyperintense FLAIR abnormality was not significantly ($P = 0.33$) different between brain infections ($91.1 \pm 72.5\,cm^3$) and necrotic GBMs ($106.9 \pm 49.8\,cm^3$). In addition, normalized $T_1$ signal intensity from contrast enhancing region was nonsignificantly ($P = 0.29$) higher in brain infections ($1.29 \pm 0.27$) that that of necrotic GBMs ($1.18 \pm 0.26$).

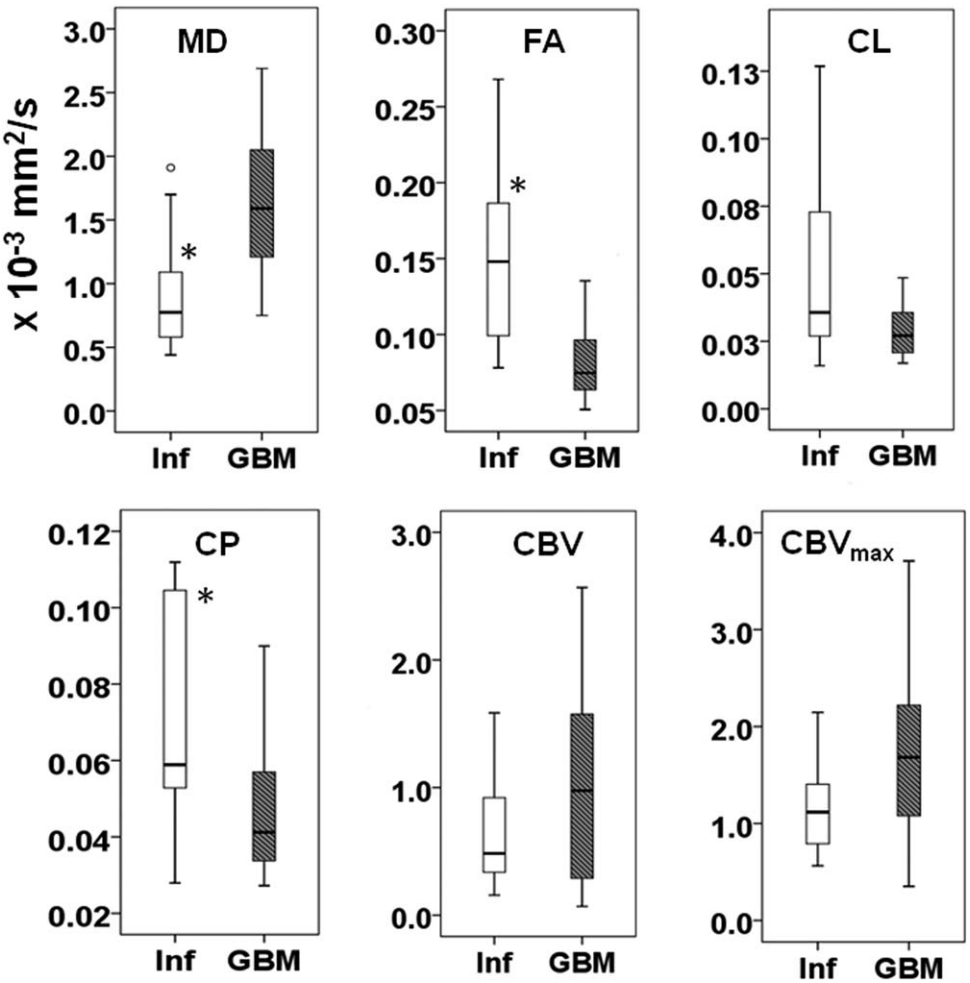


**FIGURE 4: Distribution of median values of parameters from the central core. Box-and-whisker plots from the central core of lesions demonstrate the distribution of DTI (MD, FA, CL, and CP) and DSC-PWI (rCBV and $rCBV_{max}$) parameters in distinguishing brain infections (white) and necrotic GBMs (shaded). The bottom and top edges of boxes represent the 25$^{th}$ percentile, and the 75$^{th}$ percentile values. The bands within the boxes represent 50$^{th}$ percentile (median). Whiskers display the range of data distribution. Outliers are marked with open circles (values 1.5 box length from the 75$^{th}$/25$^{th}$ percentiles). An asterisk (*) indicates significant difference ($P<0.05$) between the two groups. Significantly lower MD, higher FA, and CP were observed from the central core of brain infections compared to those of necrotic GBMs.**

## Discussion

We report the combined utility of DTI and DSC-PWI in distinguishing brain infections from necrotic GBMs in the present study. When FA from the central core and $rCBV_{max}$ from enhancing region were incorporated in multivariate logistic regression analysis, a high discriminatory accuracy was observed in differentiating brain infections and necrotic GBMs. Accurate differentiation of brain infections from necrotic GBMs is essential for planning adequate treatment and for estimating clinical outcome measures and future prognosis. However, both of these conditions may present similar clinical symptoms and analogous morphological characteristics on conventional neuroimaging[4,5] and conflicting DTI and DSC-PWI findings when these techniques are used in isolation.[14–21] In this context, our study demonstrates that brain infections and necrotic GBMs can be distinguished with high sensitivity and specificity by combined use of DTI and DSC-PWI.

Restricted diffusion in brain abscesses has been reported previously,[7,10,12] and may facilitate their differentiation from cystic brain tumors. Consistent with these previously published reports,[7,10,12] significantly lower MD values were observed from the central core of brain infections compared to those with necrotic GBMs in the present study. These findings suggest that the central core of infective and necrotic GBM lesions may harbor differential degrees of cellularity, viscosity, and cyto-architectural composition (number of inflammatory cells, protein molecules, and arrangement of collagen fibers).[12,27] However, MD from the central core provided only a moderate sensitivity of 76% and specificity of 85% in discriminating brain infections from necrotic GBMs in the present study. Moreover, this parameter was not selected in the multivariate logistic regression analysis. Collectively, these findings suggest that MD may not be a robust imaging biomarker for the differential diagnosis of these two conditions. Our finding is

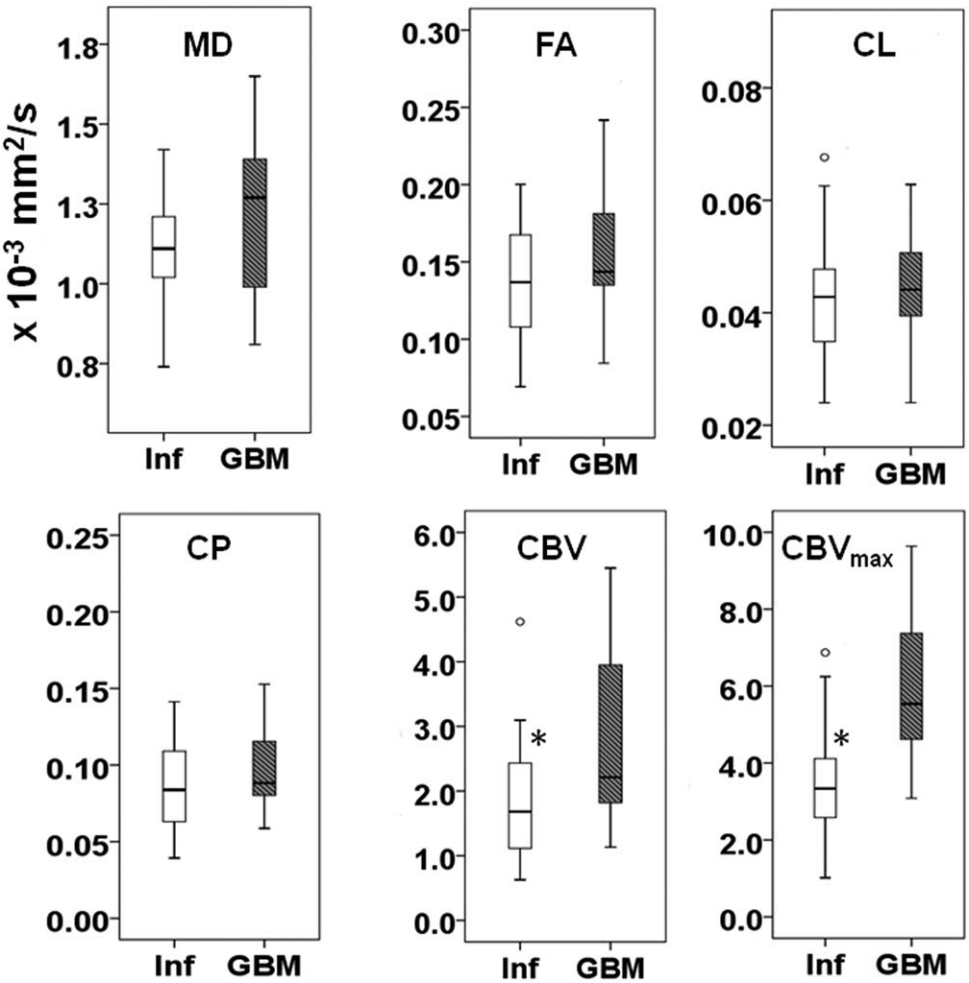


**FIGURE 5: Distribution of median values of parameters from enhancing region. Box-and-whisker plots from enhancing region of lesions demonstrate the distribution of DTI (MD, FA, CL, and CP) and DSC-PWI (rCBV and $rCBV_{max}$) parameters in distinguishing brain infections (white) and necrotic GBMs (shaded). The bottom and top edges of boxes represent the 25$^{th}$ percentile, and the 75$^{th}$ percentile values. The bands within the boxes represent 50$^{th}$ percentile (median). Whiskers display the range of data distribution. Outliers are marked with open circles (values 1.5 box length from the 75$^{th}$/25$^{th}$ percentiles). An asterisk (*) indicates significant difference ($P<0.05$) between the two groups. Significantly higher rCBV and $rCBV_{max}$ were observed from enhancing region of necrotic GBMs compared to those of brain infections.**

corroborated by earlier studies in which high diffusivity similar to that found in necrotic tumors has been reported in cases of both pyogenic and fungal abscesses that were untreated[14,15] or treated conservatively.[16] On the other hand, some other studies have also reported low MD from necrotic GBMs mimicking abscesses.[10,17]

In contrast to DWI, DTI allows estimation of anisotropic water diffusion in 3D space and DTI-derived FA parameter reflects the degree of anisotropy in a tissue.[28] In the current study, significantly higher FA from the central core of lesions was observed in brain infections than in necrotic GBMs. In a previously published case study,[29] we reported high FA from the center of an actinomycotic brain infection. Additionally, markedly elevated FA (as high as normally observed from normal white matter) have been reported from cavities of brain infections[18,19] and these FA values were significantly higher compared to those of cystic tumors.[9] It has been postulated that increased FA in abscess cavities is mainly caused by the presence of aggregated neuroinflammatory cells secondary to the release of adhesion molecules by the upregulation of antiinflammatory processes. These cell clumps become oriented and organized, resulting in high FA.[30]

A comprehensive data modeling of DTI provides additional parameters such as CL and CP describing the shape of a diffusion ellipsoid.[28] These geometric indices have been used to differentiate GBMs from brain metastases and lymphomas,[31] to differentiate classic from atypical meningiomas,[32] to characterize epidermoid cysts,[33] and brain tuberculomas,[34] suggesting that directional organization of tissue microstructures provide additional information and thus assisting in further characterization of different tissue types. Using DTI, Toh et al[9] reported significantly higher CL and CP from cystic cavities of brain abscesses than from those of necrotic GBMs, supporting the notion of accumulating branching and crossing/kissing pseudofiber structures

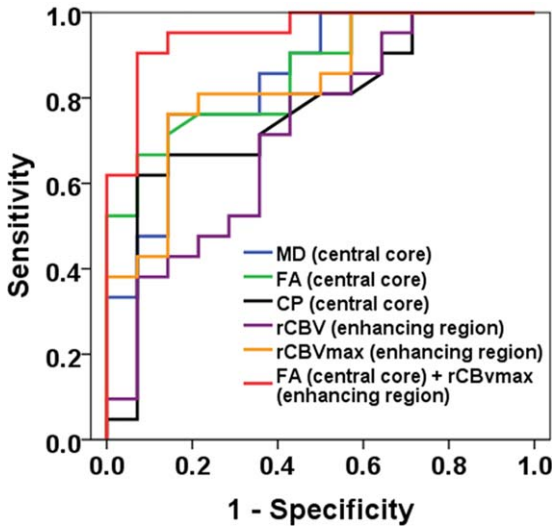


**FIGURE 6: Receiver operating characteristic (ROC) curves for individual parameters and for the best classification model. Among all individual parameters, FA from the central core was the single best predictor for distinguishing brain infections from necrotic GBM with an accuracy (AUC) of 0.86, a moderate sensitivity of 67%, and a specificity of 93% using a threshold FA value of 0.09. Incorporation of FA from the central core and $rCBV_{max}$ from enhancing region in multivariate logistic regression analyses provided the best discriminatory model to distinguish brain infections from necrotic GBMs with an AUC of 0.92, a sensitivity of 91%, and a specificity of 93%. The leave-one-out crossvalidation test revealed that 88.6% of patients were correctly classified.**

within the abscess cavity.[19,35] Congruent with this study,[9] significantly higher CP and a trend towards higher CL were observed from the central cores of brain infections than those of necrotic GBMs in the present study. Moreover, our result of showing significantly greater CP than CL from the central cores of brain infections and necrotic GBMs are in agreement with a prior study by Kumar et al[19] suggesting the presence of a planar model of diffusion tensor in these lesions. This interesting finding also provides a notion that CP had a greater contribution than CL to the increased FA from the central core of these lesions in the present study. When DTI parameters were incorporated into logistic regression and ROC analyses, MD and FA from the central core and CP from enhancing region were selected in the stepwise method, resulting in a sensitivity of 82% and a specificity of 91% in differentiating brain infections from necrotic GBMs in the present study.

Using DSC-PWI, significantly higher median rCBV and $rCBV_{max}$ were noted from enhancing regions of necrotic GBMs compared to those of brain infections in the present study. Our findings are in agreement with findings from prior studies.[6,7,11,13] The capsule of a brain abscess is primarily composed of relatively mature collagen fibers with a low capillary density[36] and hence, these lesions are generally associated with reduced rCBV, whereas high-grade tumors are characterized by neovascularization (increased microvascular density),[37] and therefore by high rCBV. When DSC-PWI parameters were incorporated into logistic regression and ROC analyses, $rCBV_{max}$ from the central core and rCBV and $rCBV_{max}$ from enhancing region were selected in the stepwise method, resulting in a sensitivity of 81% and a specificity of 86% in differentiating brain infections from necrotic GBMs. Despite these promising findings between the two types of cystic lesions in the present study, two cases of fungal abscesses demonstrated $rCBV_{max}$ greater

**TABLE 2. Area Under Receiver Operating Curves (AUC) and Associated Sensitivity and Specificity of DTI and PWI Parameters Using Logistic Regression Analyses**

| Parameter (region) | AUC | Threshold value | Sensitivity (%) | Specificity (%) |
|---|---|---|---|---|
| MD (CC) | 0.84 | $1.15 \times 10^{-3} mm^2/s$ | 76 | 85 |
| FA (CC) | 0.86 | 0.09 | 67 | 93 |
| CP (CC) | 0.77 | 0.04 | 62 | 93 |
| rCBV (ER) | 0.72 | 1.75 | 81 | 57 |
| $rCBV_{max}$ (ER) | 0.83 | 4.46 | 76 | 86 |
| Combined DTI and DSC-PWI Model FA (CC) + $rCBV_{max}$ (ER) | 0.95 | 0.52[a] | 91 | 93 |
| Only DTI Model MD (CC) + FA (CC) + CP (ER) | 0.92 | 0.48[a] | 0.82 | 0.91 |
| Only DSC-PWI Model $rCBV_{max}$ (CC) + rCBV (ER) + $rCBV_{max}$ (ER) | 0.90 | 0.70[a] | 0.81 | 0.86 |

[a]Threshold value of interaction factor from logistic regression model. CC, central core; ER, enhancing region.

than the average of $rCBV_{max}$ from all necrotic GBMs. The atypical high rCBV from the *Nocardia* brain abscess mimicking high-grade glioma has also been observed in a previous study.[20] Taken together, these unusual cases advocate the need of using a multimodality imaging protocol for differentiating brain infections from necrotic GBMs with great reliability.

By exploiting unique strengths of DTI and PWI together, several studies[22,25,31] have shown the added value of combining DTI and PWI parameters in differentiating histologic grades of gliomas, subtypes of brain tumors, and true progression from pseudoprogression conditions in patients with GBMs. When this approach was extended in the present study, backward stepwise method selected FA from the central core and $rCBV_{max}$ from enhancing region as the best variables. When these parameters were incorporated in the multivariate logistic regression analysis, a discriminatory model with a substantial high accuracy was observed in distinguishing brain infections from necrotic GBMs. Given that FA and $rCBV_{max}$ reflect inherently different physiological information, we believe that these parameters were complementary and thus interacted synergistically in the regression analysis. It is likely that this interaction might have provided greater discrimination power than what would be expected from individual parameters in the differential diagnosis.

As morphologic imaging characteristics are usually evaluated qualitatively to study brain lesions, assessment of these imaging features often remains observer-dependent, and hence may be limited by considerable user bias. In the present study, we sought to evaluate both qualitative and quantitative imaging characteristics in differentiating brain infections from necrotic GBMs. Signal intensity pattern from the central core and normalized signal intensity from contrast-enhancing regions were not significantly different between two types of lesions. Despite large variabilities seen in volumes of the central core + enhancing regions from both types of lesions, significantly smaller volumes were observed from brain infections compared to those of necrotic GBMs. However, only a moderate sensitivity of 66% and specificity of 80% were achieved in the differential diagnosis. These findings may imply that evaluations of conventional imaging features may not be reliable to distinguish brain infections from necrotic GBMs. On the contrary, techniques such as DTI and DSC-PWI are physiologically sensitive and consequently may be more accurate and reliable.

Our study is limited by a small number of brain infections. Moreover, the retrospective nature of this study might have introduced some potential bias. Despite these limitations, our findings suggest that a combined analysis of DTI and DSC-PWI data from the central cores and enhancing regions of lesions is promising in improving accuracy for distinguishing brain infections from necrotic GBMs. However, further prospective studies are warranted in a larger cohort to confirm these findings.

## References


1. Ganau L, Paris M, Ligarotti G, Ganau M. Management of gliomas: overview of the latest technological advancements and related behavioral drawbacks. Behav Neurol. 2015;2015:862634.
2. Alvis Miranda H, Castellar-Leones SM, Elzain MA, Moscote-Salazar LR. Brain abscess: current management. J Neurosci Rural Pract. 2013; 4(Suppl 1):S67–81.
3. Hakan T. Management of bacterial brain abscesses. Neurosurg Focus. 2008;24:E4.
4. Lau DW, Klein NC, Cunha BA. Brain abscess mimicking brain tumor. Heart Lung 1989;18:634–637.
5. Schwartz K, Erickson BJ, Lucchinetti C. Pattern of T2 hypointensity associated with ring-enhancing brain lesions can help to differentiate pathology. Neuroradiology 2006;48:143–149.
6. Chan J, Tsui E, Chau L, et al. Discrimination of an infected brain tumor from a cerebral abscess by combined MR perfusion and diffusion imaging. Comput Med Imaging Graph 2002;26:19–23.
7. Chiang I, Hsieh T, Chiu M, Liu G, Kuo Y, Lin W. Distinction between pyogenic brain abscess and necrotic brain tumour using 3-Tesla MR spectroscopy, diffusion and perfusion imaging. Br J Radiol 2009;82: 813–820.
8. Dorenbeck U, Butz B, Schlaier J, Bretschneider T, Schuierer G, Feuerbach S. Diffusion-weighted echo-planar MRI of the brain with calculated ADCs: a useful tool in the differential diagnosis of tumor necrosis from abscess? J Neuroimaging 2003;13:330–338.
9. Toh C, Wei K-C, Ng S-H, Wan Y-L, Lin C-P, Castillo M. Differentiation of brain abscesses from necrotic glioblastomas and cystic metastatic brain tumors with diffusion tensor imaging. Am J Neuroradiol 2011; 32:1646–1651.
10. Reiche W, Schuchardt V, Hagen T, Il'yasov KA, Billmann P, Weber J. Differential diagnosis of intracranial ring enhancing cystic mass lesions—role of diffusion-weighted imaging (DWI) and diffusion-tensor imaging (DTI). Clin Neurol Neurosurg 2010;112:218–225.
11. Erdogan C, Hakyemez B, Yildirim N, Parlak M. Brain abscess and cystic brain tumor: discrimination with dynamic susceptibility contrast perfusion-weighted MRI. J Comput Assist Tomogr 2005;29:663–667.
12. Crasto SG, Soffietti R, Rudà R, et al. Diffusion-weighted magnetic resonance imaging and ADC maps in the diagnosis of intracranial cystic or necrotic lesions: a retrospective study on 49 patients. Neuroradiol J 2007;20:666–675.
13. Muccio C, Esposito G, Bartolini A, Cerase A. Cerebral abscesses and necrotic cerebral tumours: differential diagnosis by perfusion-weighted magnetic resonance imaging. Radiol Med 2008;113:747–757.
14. Reddy JS, Mishra AM, Behari S, et al. The role of diffusion-weighted imaging in the differential diagnosis of intracranial cystic mass lesions: a report of 147 lesions. Surg Neurol 2006;66:246–250.
15. Lee E, Ahn K, Ha Y, et al. Unusual findings in cerebral abscess: report of two cases. Br J Radiol 2006;79:e156–161.
16. Cartes-Zumelzu FW, Stavrou I, Castillo M, Eisenhuber E, Knosp E, Thurnher MM. Diffusion-weighted imaging in the assessment of brain abscesses therapy. Am J Neuroradiol 2004;25:1310–1317.
17. Hakyemez B, Erdogan C, Yildirim N, Parlak M. Glioblastoma multiforme with atypical diffusion-weighted MR findings. Br J Radiol 2005; 78:989–992.
18. Gupta RK, Hasan KM, Mishra AM, et al. High fractional anisotropy in brain abscesses versus other cystic intracranial lesions. Am J Neuroradiol 2005;26:1107–1114.
19. Kumar M, Gupta RK, Nath K, et al. Can we differentiate true white matter fibers from pseudofibers inside a brain abscess cavity using

geometrical diffusion tensor imaging metrics? NMR Biomed 2008;21: 581–588.

20. Cianfoni A, Calandrelli R, De Bonis P, Pompucci A, Lauriola L, Colosimo C. Nocardia brain abscess mimicking high-grade necrotic tumor on perfusion MRI. J Clin Neurosci 2010;17:1080–1082.
21. Hakim A, Oertel M, Wiest R. Pyogenic brain abscess with atypical features resembling glioblastoma in advanced MRI imaging. Radiol Case Rep 2017;12:365–370.
22. Liu X, Tian W, Kolar B, et al. MR diffusion tensor and perfusion-weighted imaging in preoperative grading of supratentorial nonenhancing gliomas. Neuro Oncol 2011;13:447–455.
23. Prager A, Martinez N, Beal K, Omuro A, Zhang Z, Young R. Diffusion and perfusion MRI to differentiate treatment-related changes including pseudoprogression from recurrent tumors in high-grade gliomas with histopathologic evidence. Am J Neuroradiol 2015;36:877–885.
24. Wang S, Kim S, Chawla S, et al. Differentiation between glioblastomas and solitary brain metastases using diffusion tensor imaging. Neuroimage 2009;44:653–660.
25. Wang S, Martinez-Lage M, Sakai Y, et al. Differentiating tumor progression from pseudoprogression in patients with glioblastomas using diffusion tensor imaging and dynamic susceptibility contrast MRI. Am J Neuroradiol 2016;37:28–36.
26. Price SJ, Green HA, Dean AF, et al. Correlation of MR relative cerebral blood volume measurements with cellular density and proliferation in high-grade gliomas: an image-guided biopsy study. Am J Neuroradiol 2011;32:501–506.
27. Mishra AM, Gupta RK, Saksena S, et al. Biological correlates of diffusivity in brain abscess. Magn Reson Med 2005;54:878–885.
28. Le Bihan D, Johansen-Berg H. Diffusion MRI at 25: exploring brain tissue structure and function. Neuroimage 2012;61:324–341.
29. Wang S, Wolf RL, Woo JH, et al. Actinomycotic brain infection: registered diffusion, perfusion MR imaging and MR spectroscopy. Neuroradiology 2006;48:346–350.
30. Gupta R, Nath K, Prasad A, et al. In vivo demonstration of neuroinflammatory molecule expression in brain abscess with diffusion tensor imaging. Am J Neuroradiol 2008;29:326–332.
31. Wang S, Kim S, Chawla S, et al. Differentiation between glioblastomas, solitary brain metastases, and primary cerebral lymphomas using diffusion tensor and dynamic susceptibility contrast-enhanced MR imaging. Am J Neuroradiol 2011;32:507–514.
32. Wang S, Kim S, Zhang Y, et al. Determination of grade and subtype of meningiomas by using histogram analysis of diffusion-tensor imaging metrics. Radiology 2012;262:584–592.
33. Jolapara M, Kesavadas C, Radhakrishnan V, et al. Diffusion tensor mode in imaging of intracranial epidermoid cysts: one step ahead of fractional anisotropy. Neuroradiology 2009;51:123–129.
34. Gupta RK, Haris M, Husain N, Saksena S, Husain M, Rathore RK. DTI derived indices correlate with immunohistochemistry obtained matrix metalloproteinase (MMP-9) expression in cellular fraction of brain tuberculoma. J Neurol Sci 2008;275:78–85.
35. Zhang S, Bastin ME, Laidlaw DH, Sinha S, Armitage PA, Deisboeck TS. Visualization and analysis of white matter structural asymmetry in diffusion tensor MRI data. Magn Reson Med 2004;51:140–147.
36. Haris M, Gupta RK, Singh A, et al. Differentiation of infective from neoplastic brain lesions by dynamic contrast-enhanced MRI. Neuroradiology 2008;50:531–540.
37. Sugahara T, Korogi Y, Kochi M, et al. Correlation of MR imaging-determined cerebral blood volume maps with histologic and angiographic determination of vascularity of gliomas. Am J Roentgenol 1998;171:1479–1486.